Available online at www.sciencedirect.com
ScienceDirect
Journal of Solid State Chemistry 180 (2007) 679–687
JOURNAL OF SOLID STATE CHEMISTRY
www.elsevier.com/locate/jssc

Synthesis and characterization of $Ti_{1-2x}Nb_xNi_xO_{2-x/2}$ solid solutions

Mónica Martos[a,*], Beatriz Julián[a], Hakim Dehouli[a], Didier Gourier[b], Eloisa Cordoncillo[a], Purificación Escribano[a]

[a]*Departamento de Química Inorgánica y Orgánica, Universitat Jaume I, 12071, Castellón, Spain*
[b]*Laboratoire de Chimie de la Matière Condensée, CNRS-UMR 7574, 75231, Paris, France*

Received 22 September 2006; received in revised form 7 November 2006; accepted 13 November 2006
Available online 1 December 2006

Abstract

Doped-rutile has been traditionally used in ceramic pigments for its intense optical properties. In this paper, we compare the classical ceramic synthesis of $Ti_{1-2x}Nb_xNi_xO_{2-x/2}$ system with the sol–gel methodology, which allows a reduction of the anatase–rutile transformation temperature. The composition was optimised in order to obtain a unique rutile phase with the minimum amount of pollutant Ni(II) and enhanced chromatic coordinates. Incorporation of the doping ions in the rutile structure was corroborated by XRD and Rietveld refinements. The species responsible for the colour mechanism were studied by different techniques. UV–VIS spectroscopy showed the characteristic features of Ni^{2+} ions, whose existence was corroborated by EPR and magnetic measurements. From these results, (Ni,Nb)doped-TiO_2 powder samples can be now shaped as thin films, monoliths, etc. by using sol–gel methodology without modifying their properties. This study introduces new possibilities of coloured TiO_2-based solid solutions in new combined advanced applications (colouring agent and photocatalyst, etc.).

Keywords: Solid solution; Rutile phase; Sol–gel synthesis; Paramagnetic species; TiO_2-based pigments

1. Introduction

TiO_2 has attracted much attention for the last decades due to its wide industrial applications in cosmetics, paints, electronic paper, ceramics, solar cells, etc. [1]. In most of these applications TiO_2 is required as a powder, however, for specific advanced applications (optics, electronics, sensors, photocatalysis…) is convenient to shape it as films, fibers, etc. In these cases, non-conventional synthesis methods such as chemical vapour deposition, spray pyrolysis, e-gun evaporation, rf sputtering, sol–gel process, etc. must be used [2].

The allotropic structures of TiO_2 used in industry are anatase and rutile, both of them obtained as thermodynamically stable phases at higher temperatures than 400 °C. Above 1000 °C, the oxygen partial pressure increases continuously since oxygen is liberated and a partial reduction of Ti^{4+} to Ti^{3+} can occur. This phenomenon is accompanied by changes in colour and electrical conductivity. However, these changes are usually induced by substitution of Ti^{4+} by transition metal ions (Ni^{2+}, Fe^{3+}, Nb^{5+}…), which can act as chromophore species for its application in ceramics or can give excellent photocatalytic abilities [3].

As ceramic pigment, doped-rutile structures can give a wide variety of coloration. If the coloured cation substituent is not tetravalent, additional changes are needed to retain charge valence and mixed metal oxides pigments can be obtained. Among them, NiO-TiO_2 pigments have already attained a large technical application. In order to satisfy the charge valence other metal species such as Sb(V,III), Nb(V) or W(VI) can be introduced and the colouration is little affected by this second dopant [4,5]. Ni-containing rutile crystals appear more or less bright yellow shade depending on the Ni content in the solid solution but also on the nature of the co-doping ion [5]. This yellow colour is mainly

*Corresponding author. Fax: +34964728214.
E-mail addresses: mmartos@qio.uji.es (M. Martos), julian@qio.uji.es (B. Julián), didier-gourier@enscp.fr (D. Gourier), cordonci@qio.uji.es (E. Cordoncillo), escriban@qio.uji.es (P. Escribano).

0022-4596/$ - see front matter © 2006 Elsevier Inc. All rights reserved.
doi:10.1016/j.jssc.2006.11.026

caused by absorption in the blue and red regions of the spectrum of Ni(II) ions in an octahedral coordination. The co-doping of this solid solution with Sb allows the enrichment of the structure in Ni content. However, the use of Sb_2O_5 causes several problems because this oxide dissociates at ~960 °C and the oxygen is lost prior to the solid solution formation. Therefore, the volatilisation of Sb during calcination induces changes in the chemical composition [6]. Thus, the use of the other species (W, Nb) has been proposed. By doping with W, the products become darker in colour [7]. On the contrary, addition of Nb leaves the colour unchanged [8], and therefore it has been chosen as the appropriate co-dopant ion in this work.

The characteristics required for commercial uses of ceramic pigments are: colour-tone and saturation, colour covering, tinting strength, brightening and brilliance ability, non-reactivity, insolubility, chalking resistance, dispersibility, etc. [8,9]. Nowadays, Pr^{3+}-doped $ZrSiO_4$ yellow pigment is the most used for industrial glazes but this pigment is very expensive because of the high cost of its raw materials and high temperature synthesis. Therefore, research needs to be performed in developing a cheaper yellow pigment.

NiO-doped rutile has already been used in industry as an alternative yellow pigment (doped with Sb and Nb, classified as 11-15-4 and 11-16-4 DCMA [10], respectively) but it is generally prepared with a high amount of Ni ions in its composition. Nickel and its compounds represent a risk factor as they are potential carcinogens in human beings and animals, and in plants they have a phytotoxic action when present in high concentrations [11]. Since Ni species could be solubilized and removed in the washing stages, it can be an important source of pollution. The current environmental regulatory restrictions make increasingly necessary to modify the current pigmenting systems containing potential pollutants with a view to substitute and/or reduce them. As a result, diminishing the amount of nickel in Ni-containing pigments could help making ceramics a more ecological sector.

By the other hand, traditional solid-state synthesis of ceramic pigments involves slow diffusion processes because the reactants are not mixed in an atomic level. Thus, their synthesis requires high temperatures with long reaction times, which affect the economic costs and may alter the end product stoichiometry as a result of possible volatilisations during calcination. Sol–gel methodology has largely demonstrated to be a suitable synthetic procedure for preparation of ceramic pigments [12,13]. The mild conditions of sol–gel chemistry (reaction in solution, use of metalorganic precursors and organic solvents, low reaction temperatures, etc. [14]) allow the reduction of synthesis temperature and better incorporation of the doping elements, avoiding lixiviation in the washing liquids as well as the appearance of non-desired secondary phases, etc. Furthermore, the material can be shaped as a bulk, film, fibber, powder, etc [14].

Since Ni^{2+}–TiO_2 systems present other interesting properties besides its yellow coloration such as semiconducting, [15] magnetic, [16] or photocatalytic properties, [3] and the shape can be tuned in accordance with the further application, the study of sol–gel prepared $Ti_{1-2x}Nb_xNi_xO_{2-x/2}$ solid solutions with the minimum quantity of Ni(II) is crucial not only for ceramics but also as a base for new advanced applications with combined abilities.

Thus, this paper is focused on the compositional optimisation of the $Ti_{1-2x}Nb_xNi_xO_{2-x/2}$ system from an environmental point of view. Structural characteristics and optical properties of the optimised composition are compared for the material prepared by traditional ceramic and non-conventional sol–gel procedures. Finally, the oxidation states of the different elements presented in the system are studied by UV–VIS spectroscopy, EPR and magnetic measurements.

2. Experimental section

2.1. Sample preparation

Several compositions based on $Ti_{1-2x}Ni_xNb_xO_{2-x/2}$ ($x = 0.1$, 0.05, 0.03 and 0.01) stoichiometry were prepared by ceramic and sol–gel methods.

The precursors for the traditional ceramic pigment synthesis route were the corresponding oxides: TiO_2, Nb_2O_5 and NiO. In this method, the reactants were mixed and homogenised by wet milling with acetone in a planetary ball mill for 20 min. The heat treatment was chosen from similar ceramic studies [12] in which good colorations are developed at 1200 °C. Thus, samples were fired in air at 1200 and 1300 °C with annealing times of 2 and 6 h in a Nabertherm electric furnace at a heating rate of 10 °C/min. After heat treatment, samples showed yellow coloration. To refine and homogenise the particle size after calcination, the resulting products were ground in an agate mill with acetone.

The samples were also prepared by sol–gel procedure. This process is based on the hydrolysis and condensation of the corresponding metal precursors. Firstly, titanium (IV) isopropoxide, niobium (V) ethoxide and nickel (II) nitrate hexahydrate were separately dissolved using absolute methanol and then were mixed leading to a transparent solution. After a complete homogenisation, the sol was dried and a transparent monolith was obtained, as shown in Fig. 1. The samples were ground and calcined in the same way that the ceramic samples.

2.2. Characterization techniques

Phase analysis of the fired samples was performed by X-ray powder diffraction (XRD) with a SIEMENS D5000 diffractometer with Cu $K\alpha$ radiation. Data were collected by step-scanning from 20 to 70°2θ with a step size of 0.05°2θ and 5 s counting time at each step. The goniometer was controlled by the "SIEMENS DIFFRACT plus"

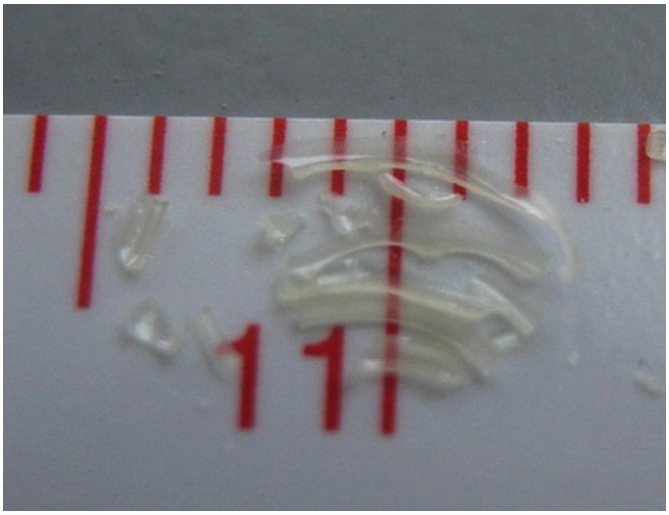

Fig. 1. Photography of the sol–gel sample with composition $Ti_{0.98}Nb_{0.01}Ni_{0.01}O_{1.995}$.

software, which also determined diffraction peak positions and intensities. The instrument was calibrated using an external Si standard.

For Rietveld analysis, powder XRD patterns were collected over 2θ range from 10° to 110°, the step scan was selected with step width of 0.02° and scanning time of 10 s. The refinement of structure was carried out by using the FULLPROF program, developed by Rodriguez-Carvajal [17]. The structural model and initial structural parameters for $Ti_{1-2x}Nb_xNi_xO_{2-x/2}$ ($x = 0.01$) were taken as follows: space group $P4_2/mnm$; Ti(IV), Nb(V) and Ni(II) were in the Wyckoff 2a and O^{2-} ions in the 4*f* positions. Diffraction profiles were modelled by using a pseudo-Voigt function that was corrected for peak asymmetry for angles less than 40°2θ. The final refinement converged to give R_F and R_{Bragg}. The refined crystallographic parameters were: scale factors, zero point, six parameters for the background, rutile cell dimensions, atomic positions, peak asymmetry and the overall isotropic displacement temperature factor.

UV–visible–NIR spectroscopy and a colorimetric study of the samples were carried out in a CARY 500 SCAN VARIAN spectrophotometer in the 300–1100 nm range. The diffuse reflectance spectra (DRS) were obtained using an integrating sphere and $BaSO_4$ as reference. The CIELAB colour parameters $L^*a^*b^*$ were determined by coupling an analytical software for colour measurements to the VARIAN spectrophotometer. The data were registered from 380 to 700 nm using a PTFE blank as reflecting standard and a D65 standard illuminant. The chromatic coordinates of the samples have been compared with those of a commercial yellow pigment used in the ceramic industry. In the CIELAB system, L^* is the lightness axis [black (0) to white (100)], a^* is the green (<0) to red (>0), and b^* is the blue (<0) to yellow (>0) axis. [9,18]

The study of Ni content in the washing liquids of the samples was realized by an induced coupled plasma (ICP-MS). For this analysis, 0.3 g of the fired sample was subjected to successive washings with hot 0.3 M HNO_3, and the Ni content in these acid washing liquids was directly measured.

Scanning electron micrographs of the samples were taken on a scanning electron microscope (SEM) Leica, Leo 440 model, equipped with a spectrometer of energy dispersion of X-ray (EDX) from Oxford instruments, using the following operational parameters: acceleration voltage 20 kV, measuring time 100 s, working distance 25 mm, counting rate 1.2 kcps. The samples for microstructural and microanalysis determinations were deposited in an aluminium holder and coated by graphite film.

Particle size was measured in a Coulter LS230 with micro volume module. The particle-size range which can be determined by this instrument lies between 0.4 and 2000 μm.

Electron paramagnetic resonance (EPR) measurements were performed with an X-band Bruker Elexsys E 500 spectrometer equipped with Oxford Instrument variable temperature device. The spectra were recorded at 9.5 GHz with a microwave power of 20 mW and magnetic field modulation amplitude of 0.5 mT.

Magnetic susceptibility of the polycrystalline samples was obtained using a Quantum Design SQUID magnetometer in the temperature range 1.9–300 K and magnetic fields from 50 G to 1 T. magnetisation measurements were carried out at 2.0 K operating up to 5 T. Sealed plastic bags of about 5 mg were used as sample containers. The susceptibility data were corrected according to the diamagnetism of the container and the sample (40.10^{-6} cm^3 mol^{-1}). Susceptibility is represented as molar susceptibility using a molecular weight of 79.9 g/mol, corresponding to TiO_2.

3. Results and discussion

3.1. Compositional study

Firstly, a preliminary study was made in order to optimise the solid solution stoichiometry and the annealing temperature regarding the best coloration. The samples studied in this initial study were the ones synthesised by the ceramic route.

Fig. 2 illustrates the XRD patterns obtained for the different $Ti_{1-x}Nb_xNi_xO_{2-x/2}$ compositions fired at 1200 °C/2 h, revealing the formation of the rutile phase (JCPDS 87–710).

A secondary phase associated to $NiTiO_3$ (JCPDS 76–334) was found in all the solid solutions except for the $x = 0.01$ composition, in which the rutile phase appears as a single phase. In this sample, Ni ions seem to be completely incorporated into the rutile lattice, giving the $Ti_{0.98}Nb_{0.01}Ni_{0.01}O_{1.995}$ solid solution. The existence of this solid solution is supported by the shift observed for the peak positions towards lower 2θ values. The cell parameters of the rutile lattice for the non-doped and doped ($x = 0.01$) samples have been obtained from the

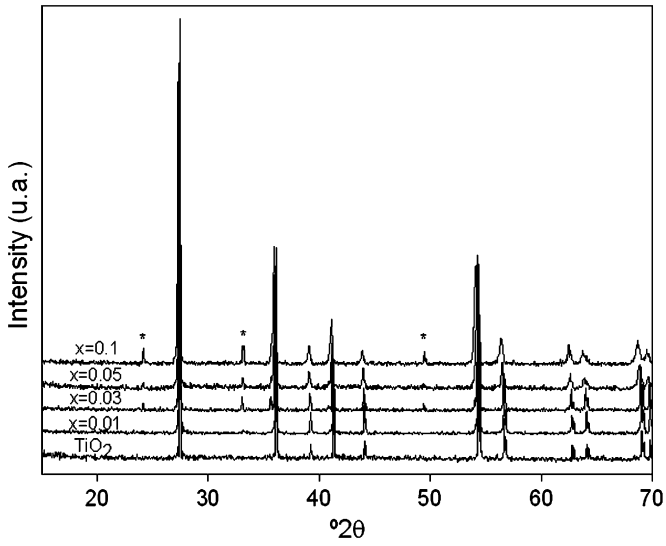

Fig. 2. XRD spectra for the ceramic samples calcined at 1200 °C/2 h. (*: indicates the $NiTiO_3$ secondary phase, JCPDS 76–334).

Table 1
Cell parameters obtained for ceramic and sol–gel $Ti_{0.98}Nb_{0.01}Ni_{0.01}O_{1.995}$ samples at different temperatures

$Ti_{0.98}Nb_{0.01}Ni_{0.01}O_{1.995}$	Ceramic		Sol–gel	
	a	*c*	*a*	*c*
900 °C	*	*	4.5939	2.9608
1000 °C	4.5943	2.9594	4.5942	2.9607
1100 °C	4.5945	2.9598	4.5943	2.9611
1200 °C	4.5957	2.9603	4.5947	2.9618
1300 °C	4.5967	2.9612	4.5958	2.9624

*Indicates the presence of anatase and rutile TiO_2 phases.

adjustment of the XRD patterns with the WinXPow program. The *a* and *c* cell parameters increase from 4.5906 to 4.5957 Å and from 2.9581 to 2.9603 Å, respectively, with incorporation of the dopant elements after calcination at 1200 °C. This expansion of the lattice agrees with the substitution of Ti ions in their atomic positions by Ni and Nb ions, since the atomic radii for Ti^{4+} (74.5 pm) is smaller than those of the dopants in octahedral coordination (Ni(II): 83 pm and Nb(V): 78 pm) [19]. In the case of samples with $x \geqslant 0.03$ the increase of the cell parameters is still observed (e.g. for $x = 0.03$, $a = 4.6018$ Å and $c = 2.9638$ Å), but the apparition of a secondary phase certainly influences the solid solution formation.

The effect of the heating temperature (from 900 to 1300 °C) on the rutile lattice has also been studied for the composition with $x = 0.01$ and the data are resumed in Table 1. A feeble increase of both *a* and *c* parameters with the temperature can be observed, indicating that the lattice still incorporates dopant ions because of the more facilitated diffusion processes. The increase of the *a* parameter is higher than that of the *c* parameter, indicating a distortion of the structure with the doping.

The effect of the soaking time was also evaluated by XRD but the variations in the crystalline phases and cell parameters were less important than the effect of composition and temperature and the results were not worthy to be mentioned here.

Fig. 3(a) depicts the b^* chromatic coordinate, which indicates the yellow contribution and the Ni content in the washing liquids obtained for the powder samples. The b^* coordinate of a commercial yellow pigment (dotted line, standard:std) based on Pr-doped $ZrSiO_4$ is included as a reference of the typical coloration used in industry. Taking into account that the sample with $x = 0.01$ was the only one showing TiO_2 as single phase, the best b^* value for this composition was obtained after firing at 1200 °C/2 h. Moreover, for this specific thermal treatment the b^* value was not very sensitive to the composition, what is of great interest from an industrial application point of view. Even if some samples with higher content in Ni ($x \geqslant 0.03$) showed a better yellow coloration, the much higher Ni content in the washing liquids (see Fig. 3(b)) and the appearance of a secondary phase make the $x = 0.01$ stoichiometry the optimal composition from an environmental point of view.

The pigments were tested in commercial glazes and all of them resulted to be stable after a standard industrial ceramic tile firing cycle.

3.2. Ceramic vs. sol–gel procedure

Once the optimal composition ($x = 0.01$) was chosen, it was compared with the sol–gel route synthesis. As this methodology allows a higher reactivity, the anatase–rutile transformation should occur at low temperatures. Indeed, (Ni,Nb)-doped rutile single phase was obtained after heat treatment at 900 °C for 2 h with intense yellow coloration ($L^* = 79.4$, $a^* = 0.1$ and $b^* = 45.6$). On the contrary, the sample synthesised by ceramic procedure did not develop either a single rutile phase or yellow coloration at 900 °C ($L^* = 87.5$, $a^* = -2.3$, $b^* = 15.0$). Thus, this kind of sol–gel materials would be interesting for industrial applications at low temperatures. However, although the sol–gel sample presented yellow coloration with good stability within a standard glaze (firing cycle at 1080 °C), it has been preferred to calcine the sol–gel pigment at 1200 °C/2 h in order to compare its properties with those of the ceramic one. The XRD pattern is shown in Fig. 4, and it presents the same features than that of ceramic sample, i.e. a single rutile phase and a shift of the diffraction peaks because of the incorporation of Ni(II) and Nb(V) in the rutile lattice.

The structural study of the sol–gel $Ti_{0.98}Nb_{0.01}Ni_{0.01}O_{1.995}$ solid solution with temperature was also performed by adjusting the XRD patterns with the WinXPow program, and the variation of the *a* and *c* rutile cell parameters are resumed in Table 1. The effect in the parameters was the same that for ceramic samples, i.e. the expansion of the lattice with temperature.

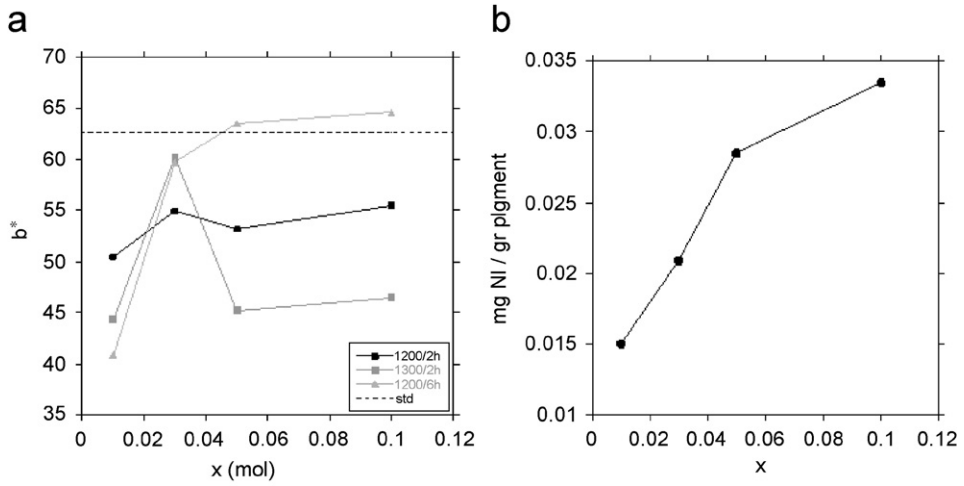

Fig. 3. (a) Colorimetric coordinates of ceramic samples and (b) Ni content in washing liquids of samples fired at 1200 °C/2 h.

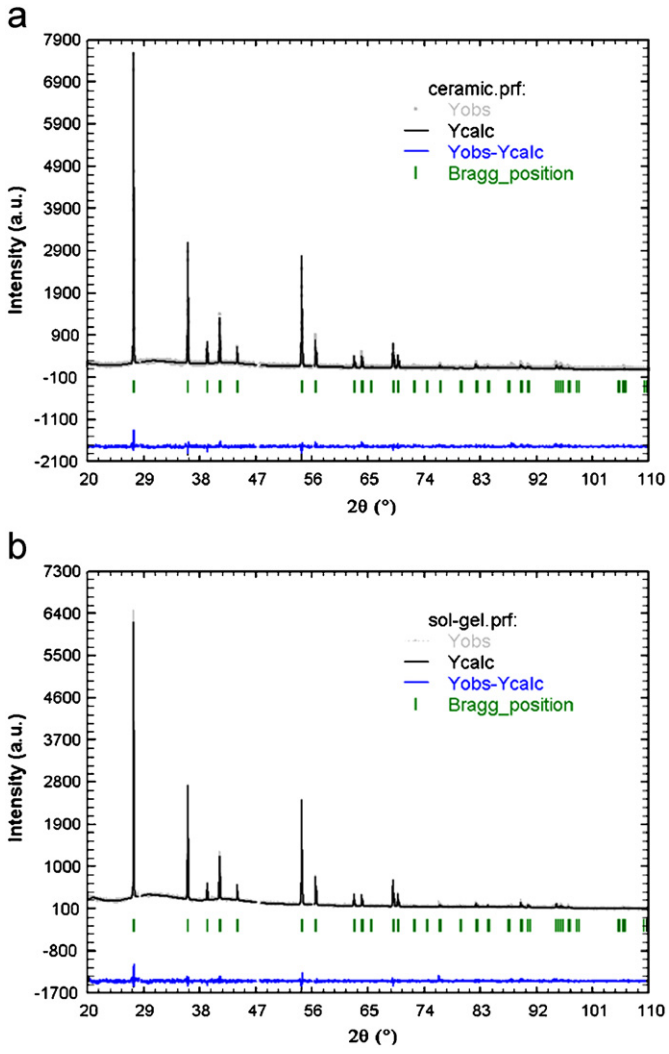

Fig. 4. Calculated (the top solid line) and observed (the cross markers) X-ray diffraction pattern for $Ti_{0.98}Nb_{0.01}Ni_{0.01}O_{1.995}$ (a) ceramic sample and (b) sol–gel sample. The lowest line represents the difference between the calculated and observed intensities. The vertical markers stand for the angles of Bragg reflections. Results of fit using the space group $P42/mnm$.

Table 2
Chromatic coordinates and Ni content in the washing liquids for samples with $x = 0.01$ fired at 1200 °C/2 h

Sample	L^*	a^*	b^*	mg Ni/gr pigment
Ceramic	76.5	2.4	50.4	0.015
Sol–gel	82.9	−2.1	51.8	0.013

Chromatic coordinates and the Ni content in the lixiviated liquids (expressed as mg of Ni per gram of pigment) for both synthesis methods are resumed in Table 2. It can be observed that the chromatic coordinates are very close and that the Ni segregation in the sol–gel sample is lower than in the ceramic one.

With the aim of comparing the incorporation of Ni and Nb ions in the rutile structure in ceramic and sol–gel synthesis, an accurate study by the Rietveld method of the optimised samples was made. The structural refinement patterns for the doped ceramic and sol–gel samples are included in Fig. 4.

The final Bragg factor R_B for the two samples was 8.974% and 7.429%, respectively. The quality factors (GoF) for both samples were obtained from

$$GoF = \frac{R_{wp}}{R_{exp}},$$

where R_{wp} and R_{exp} are the weighted residual error and the expected error, respectively. The calculated GoF values were 1.18 and 1.14 for ceramic and sol–gel samples, indicating a good fit adjustment. The cell parameters, as already mentioned, evidenced a significant increase in the cell volume of the doped samples ($V_{ceramic} = 62.52\,Å^3$ and $V_{sol-gel} = 62.50\,Å^3$) in comparison with the non-doped structures ($V_{ceramic} = 62.34\,Å^3$ and $V_{sol-gel} = 62.35\,Å^3$). It is important to note that the non-doped ceramic and sol–gel samples were prepared following the same

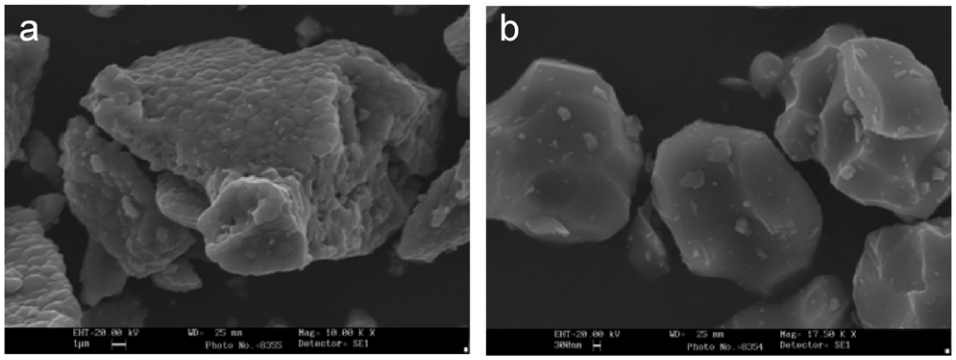

	TiO_2	NiO	Nb_2O_5
1	96.99	0.58	2.43
2	96.42	0.58	3.00
3	96.34	0.42	3.24

	TiO_2	NiO	Nb_2O_5
1	97.18	0.67	2.15
2	94.87	1.13	4.00
3	97.54	0.48	1.97

Fig. 5. SEM micrographs and EDX results of (a) sol–gel sample; (b) ceramic sample.

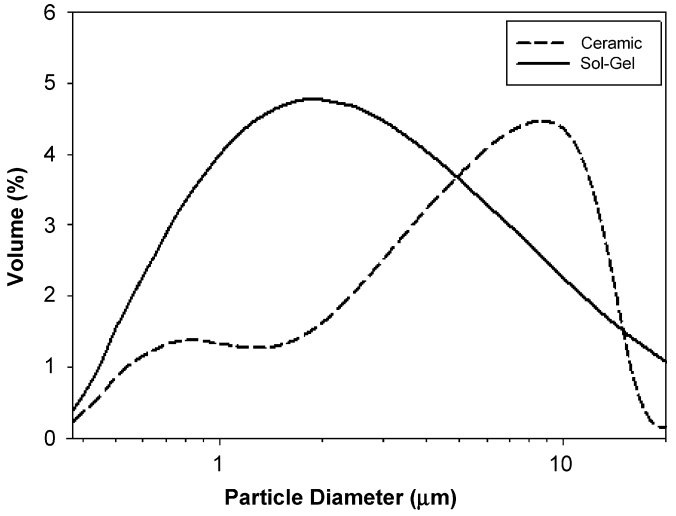

Fig. 6. Particle size analysis of ceramic and sol–gel samples.

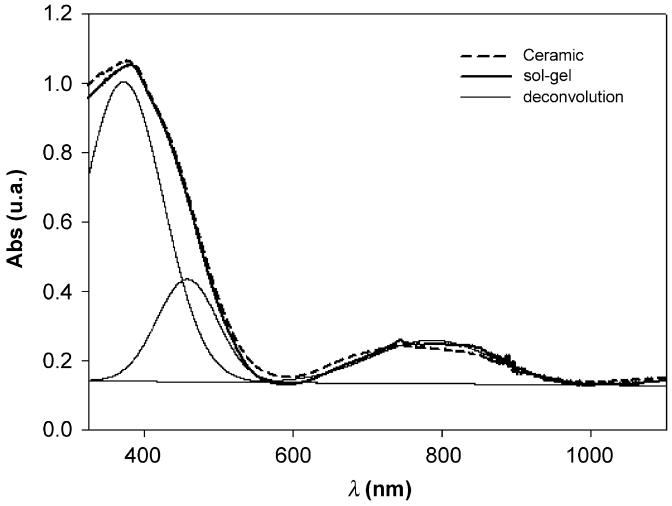

Fig. 7. UV–Vis spectra for the ceramic and sol–gel samples. As an example, deconvolution of sol–gel spectrum is also included.

experimental protocol. These results corroborate once again the distortion of the rutile host structure because of the introduction of the doping ions (with larger sizes than titanium ions).

Particle size is known to be an important parameter which strongly influences powder characteristics (coloration, stability in the glaze, etc.). Fig. 5 shows some photographs obtained by SEM and the semi-quantitative analysis made by EDX of ceramic and sol–gel samples. In both cases, particle sizes are found in the micrometric scale, which is characteristic of the high firing temperatures. Ceramic particles do not present any specific morphology meanwhile the sol–gel ones are constituted by aggregation of small grains. Elemental analysis by EDX indicated that the chemical compositions were close to stoichiometrical percentages (97.42% TiO_2, 0.93% NiO and 1.65% Nb_2O_5). Moreover, as shown in Fig. 6, the maximum of the particle size distribution for the sol–gel sample appears at lower value than that obtained for the ceramic one. These results are in accordance with the grain size observed in the SEM photographs. As a conclusion, in this study, the presence of small grains in sol–gel particles does not significantly influences the coloration after calcining at 1200 °C, but could contribute to the lower Ni lixiviation observed in the sol–gel pigment.

3.3. Study of the colour mechanism

To the best of our knowledge, no information about the colour mechanism of the $Ti_{1-2x}Nb_xNi_xO_{2-x/2}$ system has been reported. In order to go deep in this matter, a study by UV–VIS spectroscopy, EPR and magnetic measurements was performed.

The DRS patterns are depicted in Fig. 7, and show very similar features. In order to determine the position of the

bands, deconvolution of the spectra was performed. As an example, Fig. 7 includes the different components obtained for the spectrum of the sol–gel sample. Both spectra show the characteristic bands of Ni^{2+} in the rutile structure. Two strong absorbance bands at ~27,000 and ~22,000 cm^{-1} are attributable to the $Ti^{4+} \leftrightarrow O^{2-}$ charge transfer and to the v_3 transition $^3A_{2g}(^3F) \rightarrow {}^3T_{1g}(^3P)$ of the Ni^{2+} ion in an octahedral field, respectively. The maximum light transmission at around 17,000 cm^{-1} justifies the intense yellow colour of these pigments. A less intense broad peak centred at the red-NIR border (at ~13,000 cm^{-1}) is observed, and it can be assigned to the v_2 transition $^3A_{2g}(^3F) \rightarrow {}^3T_{1g}(^3F)$ of the Ni^{2+} ion in an octahedral field [20,21]. In the red-NIR region there is another peak at ~13,500 cm^{-1}, that could be due either to the unusual co-presence of Ni^{3+}, $^4T_{1g}(^4F) \rightarrow {}^4T_{2g}(^4F)$, or to a considerable splitting of the Ni^{2+} v_2 transition, as wide as 11,900–14,100 cm^{-1}, related to the TiO_6 octahedral transition [7]. These features are further studied by EPR and magnetic measurements.

It is well known that Ti(IV) tends to reduce into Ti(III) giving light yellow shade. In order to determine the possible presence of other active species besides Ni^{2+} ions responsible for the coloration, EPR analysis at different temperatures was performed.

Two representative EPR spectra found for the ceramic and sol–gel samples at 30 K and 10 K are depicted in Figs. 8 and 9. The response observed in both samples is quite similar, indicating that the type of paramagnetic species is the same. At temperatures $\geqslant$30 K (Fig. 8) the spectra are composed of one intense signal which can be associated to the existence of Ni(II) in a very symmetric coordination (Oh) or Ni(III). The position of the signal presence of Nb(IV) and Ti(III) is completely discarded. An interesting behaviour is observed when the temperature reaches values below 30 K (see Fig. 9). The magnetic response drastically diminishes, contrarily to the Curie's law. This effect can be due to the existence of ferro- or antiferromagnetic interactions between the spins of neighbour magnetic species.

In order to prove the EPR results about the existence of Ni^{3+} ions, a complementary study of magnetic behaviour of the samples was performed. The magnetic properties of the samples expressed as $\chi_M T$ vs. T (χ_M being the molar magnetic susceptibility) are displayed in Fig. 10(a). $\chi_M T$ at room temperature is around 0.013 $cm^3\,mol^{-1}\,K$ for both ceramic and sol–gel samples. If we consider that the magnetic response is generated from Ni (II) as the unique oxidation state, with $S = 1$ and $g = 2.2$, this $\chi_M T$ value would be associated to the presence of ~0.01 Ni(II), which is completely in agreement with the initial proposed stoichiometry. On the contrary, if the nickel introduced in the samples is completely oxidised to Ni(III), with $S = 1/2$ and $g = 2.2$, the expected susceptibility value would be around 0.45 $cm^3\,mol^{-1}\,K$. This value would correspond to 0.029 Ni molar ratio in the stoichiometric formula, which is far from the prepared composition. Since EPR experiences evidenced the existence of Ni(III) species, the low total magnetisation of the samples indicates that this specie must be in a very small quantity. In the same way, the presence of another paramagnetic such as Ti(III) would also give high susceptibility values (~0.36 cm if all Ti species are in this oxidation state, with $S = 1/2$ and $g = 1.96$), which is not the case. Furthermore, its existence has been discarded by EPR measurements.

An important feature is that at low temperature, the existence of antiferromagnetic interactions between

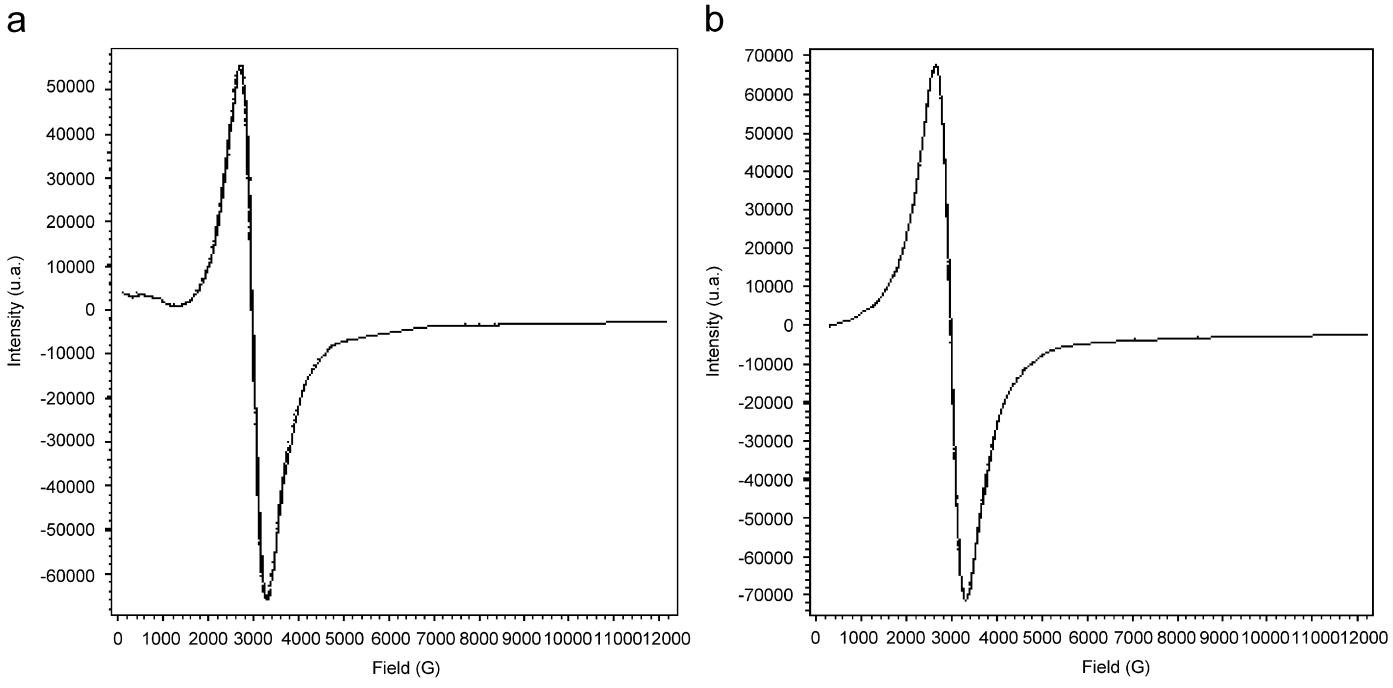

Fig. 8. EPR spectra at 30 K (a) ceramic sample and (b) sol–gel sample.

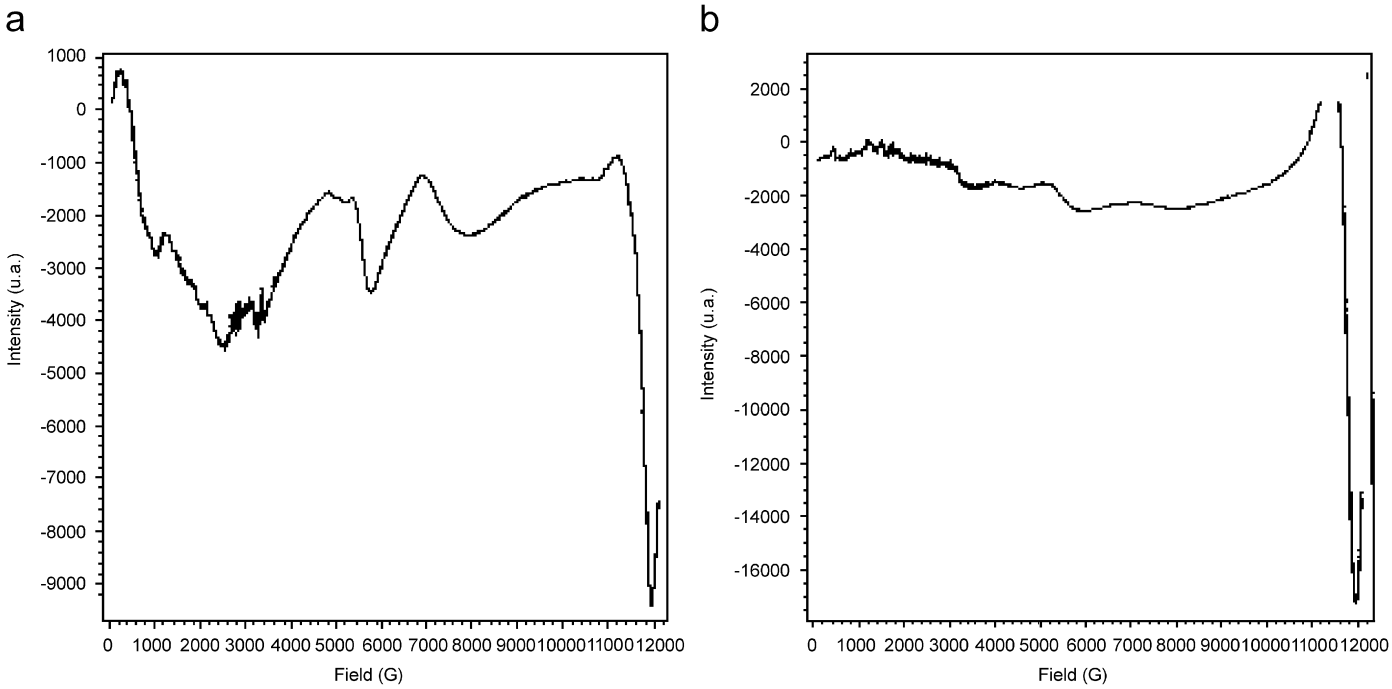

Fig. 9. EPR spectra at 10 K (a) ceramic sample and (b) sol–gel sample.

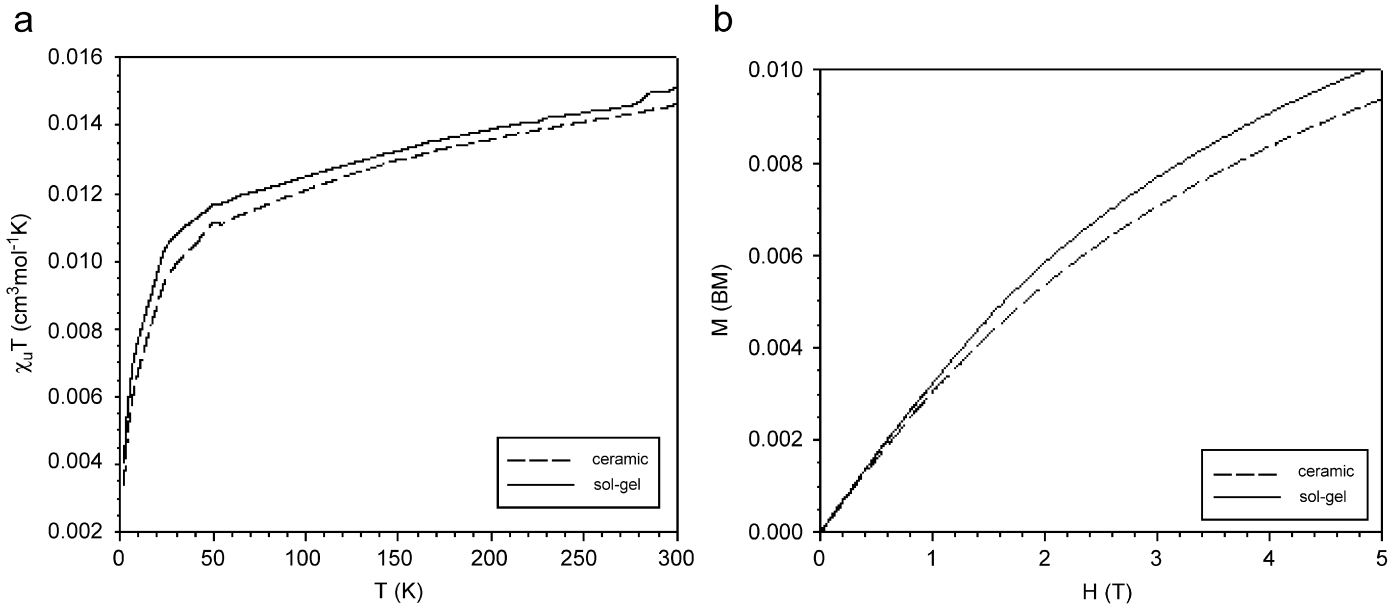

Fig. 10. Magnetic measurements of ceramic and sol–gel samples. (a) magnetic susceptibility as function as temperature and (b) magnetisation analysis vs. magnetic field.

paramagnetic ions can be observed, what is in agreement with the diminution of the magnetic response previously detected by EPR.

Fig. 10(b) shows the magnetisation vs. magnetic field recorded at 2 K. In this figure no saturation is reached after application of 5 T, which corroborates the presence of antiferromagnetic interactions at low temperature. However, saturation can be expected at values higher than 0.015 MB. If all Ni species appear as Ni(II) the saturation would be at about 0.020 MB; meanwhile a saturation value of 0.011 MB would be expected for Ni(III) as the only ion, being this last possibility discarded by the experimental results.

From this study it can be concluded that the origin of the colour could be associated to the incorporation of Ni^{2+} ions in the octahedral positions of the rutile structure.

4. Conclusion

In summary, we report the synthesis of $Ti_{1-2x}Nb_xNi_xO_{2-x/2}$ by sol–gel route in comparison to traditional solid-state process, allowing the reduction of the yellow pigment synthesis temperature up to 300 °C. The analysis of the structure, the coloration power and magnetic properties of the optimised composition ($x = 0.01$) at 1200 °C indicated a similar behaviour independently of the experimental procedure. The incorporation of Nb(V) and Ni(II) doping ions in the rutile structure was corroborated by XRD and Rietveld refinements. Chromatic coordinates, specially the yellow component, resulted to be very similar, and Ni content in the washing liquids was lightly lower in the case of sol–gel pigment. The colour mechanism was investigated by UV–VIS spectroscopy, EPR and magnetic measurements, and we concluded that Ni^{2+} was the main specie responsible for the yellow coloration. The resemblance observed in the $Ti_{0.98}Nb_{0.01}Ni_{0.01}O_{1.995}$ characterization prepared by both routes is a very important result from a technological point of view. Thus, the doped-TiO_2 powder samples, traditionally obtained by ceramic process, can be now prepared as thin films, monoliths, etc. by using the sol–gel methodology without modifying their properties. This study introduces new possibilities of coloured TiO_2-based solid solutions, not only in the field of ceramic pigments but also in new combined advanced applications (colouring agent and photocatalyst, etc.).

Acknowledgment

This research was supported by the Spanish Government (Ministerio de Educación y Ciencia: MAT-2005-00541) and Bancaixa Foundation-Universitat Jaume I (P1-1B2003-27) Projects. M. Martos and B. Julián specially thank to UJI and MEC for their PhD and postdoctoral grants, respectively.

References

[1] D.S. Hwang, N.H. Lee, D.Y. Lee, J.S. Song, S.H. Shin, S.J. Kim, Smart Mater. Struct. 15 (2006) S74.
[2] S.D. Park, Y.H. Cho, W.W. Kim, S-J. Kim,, J. Solid State Chem. 146 (1999) 230.
[3] J.M. Benlloch, J. Isasi, M. López, M.L. Veiga, C. Pico, S. Fischer, W. Gopel, J. Mater. Sci. 31 (1996) 6609.
[4] F. Hund, Angew. Chem. Int. Ed. 1 (1962) 41.
[5] S. Sorli, M.A. Tena, J.A. Badenes, J. Calbo, M. Llusar, G. Monrós, J. Eur. Ceram. Soc. 24 (2004) 2425.
[6] H.B. Krause, Mater Res. Bull. 3 (1968) 241.
[7] M. Dondi, G. Cruciani, G. Guarini, F. Matteucci, M. Raimondo, Ceram. Int. 32 (2006) 393.
[8] G. Buxbaum, Industrial Inorganic Pigments, Wiley-VCH, New York, 1997.
[9] P. Escribano, J.B. Carda, E. Cordoncillo, Esmaltes y Pigmentos Cerámicos, Enciclopedia Cerámica (3er Tomo) Ed. Faenza Editrice Ibérica, 2001.
[10] DCMA, Classification and Chemical description of the Mixed Metal Oxide Inorganic Colored Pigments, Metal Oxides and Ceramic Colors Subcommittee, second ed., Dry Color Manufacturer's Ass., Washington, DC, 1982.
[11] [a] E. Denkhaus, K. Salnikow, Crit. Rev. Oncol./Hematol. 42 (2002) 35;
[b] K.S. Kasprzak, F.W. Sunderman, K. Salnikow, Mutat. Res./Fund. Mol. Mech. Mutagen. 533 (1–2) (2003) 67.
[12] R. Muñoz, M. Martos, C.M. Rotaru, H. Beltrán, E. Cordoncillo, P. Escribano, J. Eur. Ceram. Soc. 26 (2006) 1363.
[13] B. Julián, H. Beltrán, E. Cordoncillo, P. Escribano, J.V. Folgado, M. Vallet-Regí, R.P. del Real, Eur. J. Inorg. Chem. (2002) 2694.
[14] C.J. Brinker, G.W. Scherrer, Sol–Gel Science. The Physics and Chemistry of Sol–Gel Processing, Academic Press, San Diego, 1990.
[15] J.M. Belloch, J. Isasi, M.L. López, M.L. Veiga, C. Pico, Mater. Res. Bull. 29 (1994) 861.
[16] E. Ramos, M.L. Veiga, F. Fernández, R. Sáez-Puche, C. Pico, J. Solid State Chem. 91 (1991) 113.
[17] J. Rodríguez-Carvajal, FullProf program, February 2005-LLB-LCSIM, Laboratoire Leon Brillouin, CEA-CNRS, France.
[18] E.J. Dilabert, Medida del color, Servicio de Publicaciones, Madrid, Spain, 1982.
[19] R.D. Shannon, C.T. Prewitt, Acta Crystallogr. Sect. A 32 (1976) 751.
[20] A.S. Marfunin, Physics of Minerals and Inorganic Materials. An introduction,, Springer, Berlin, 1979.
[21] M. Wildner, M. Andrut, C.Z. Rudowicz, EMU Notes Mineral 6 (2004) 93.